RSC Advances

ROYAL SOCIETY OF CHEMISTRY

www.rsc.org/advances

Synthesis of new kind of macroporous polyvinyl-alcohol formaldehyde based sponges and its water superabsorption performance

Yanxiong Pan, Kai Shi, Zhi Liu, Weicai Wang, Chao Peng, XianglingJi*

State Key Laboratory of Polymer Physics and Chemistry, Changchun Institute of Applied Chemistry, Chinese Academy of Sciences, Changchun 130022, P. R. of China

Abstract

Novel superabsorbents based on hydrophilic and macroporous polyvinyl alcohol-formaldehyde (PVF) sponges are prepared through the grafting polymerization of hydrophilic acrylamide (AM) monomer on the PVF and PVF-GA (pre-crosslinked with glutaradehyde) network and through subsequently partial hydrolysis under alkaline conditions. Attenuated total reflection infrared spectroscopy (ATR-IR) and Solid-state CP/MAS ^{13}C-NMR spectra confirm that these processes have successfully occurred. The grafting percentage (*GP*) increases with the feed ratio of [AM]/[OH] and can reach up to 160%. The hydrolysis degree ranges between 60% and 70%. Similar to the pure PVF sponges, as-prepared polyacrylamide grafted PVF (PVF-g-PAM) and PVF-GA (PVF-g-GAM), and corresponding hydrolyzed samples (PVF-g-PAA and PVF-g-GAA) present average pore sizes ranging from 60 μm to 90 μm and a high porosity of 90%, as measured using a mercury intrusion porosimeter. Scanning electron microscopy (SEM) images reveal interconected pore structure,

macroscopically rough surface, and pore size ranging from a several micrometer to 200μm. As-prepared sponges also exhibit rapid absorption kinetics and they can reach absorption equilibrium in both deionized water and saline solution in 1 min. These features are attributed to the hydrophilic surface, high porosity and interconnected pore structure. The absorption procedure described in this study is consistent with the pseudo second-order rate kinetic equation. Notably, the PVF-g-PAA sponges can absorb deionized water as high as 320g·g^{-1} within 60 s and can also absorb saline solution at a maximum capacity of 97.3 g·g^{-1} in 30 s. As-prepared PVF-g-PAM sponges with absorption capacity less than 50 g·g^{-1}exhibit excellent reusability at least for 20 cycles, this property is realized through simple squeezing. And the absorption mechanism is also discussed. Results show that these sponges with rapid absorption kinetics and high capacity can be considered as new superabsorbents for medical and sanitary applications.

Introduction

Hydrogels, containing structurally crosslinked hydrophilic polymers, such as polyacrylamide and polyacrylic acid, have been extensively investigated for applications such as absorbents[1, 2], tissue engineering materials[3] and drug delivery system[4]. However, the slow swelling rate of conventional superabsorbents that require several hours, or even days, to reach adsorption equilibrium limits the applications of these materials in multiple areas. In general, decreasing the characteristic size of dried superabsorbents is an effective approach to improve water absorption kinetics. Thus, conventional superabsorbents are commonly prepared into small particles, rods or sheets to minimize the diffusion length of absorbed water. The dependence of the swelling rate of hydrogels on size and shape hinders the applications of these substances, especially for large monoliths[5-8]. In another effective strategy, an interconnected pore structure is incorporated into a polymeric hydrogel network.

Superporous absorbents, which were first reported by Chen *et al*[9], exhibit rapid swelling and responsive properties because water is absorbed through capillary pressure via interconnected pores. Superporous absorbents or macroporous hydrogel with open-cell structure in the polymer network could effectively reduce the time to reach absorption equilibrium and maintain the monolith structures, which display certain advantages such as greater structural integrity and relatively higher mechanical properties than the conventional hydrogels of small particle[10]. These superporous absorbents with different structures and properties can be obtained using various monomers such as acrylamide[11], acrylic acid[12], sodium acrylate[13], 3-sulfopropyl

acrylate-potassiumsalt (SPAK)[14] and NIPAAm[15, 16]; these absorbents can also be prepared through various methods, including phase separation[10], porogen, ice-template and emulsion crosslinking. The swelling rate is mainly determined by the pore structures of hydrogels, and the swelling degree is controlled by chemical composition and crosslinking degree. Furthermore, the grafting polymerization is a simple and effective approach to substantially modify the chemical composition and obtain hydrogels with high absorption capacities. For example, sodium acrylate and 1-vinyl-2-pyrrolidone grafted chitosan[17], poly (acrylic acid-co-acrylamide) grafted chitosan[18], starch-g-polyacrylamide/mineral powder[19] sodium acrylate-grafted guar gum[20, 21] and modified rectories[22] are used to modify hydrogels. Indeed, the presence of hydrophilic polymer or a polyelectrolyte in a hybrid material can effectively enhance the swelling degree of original material in water.

Traditional hydrophilic and macroporous polyvinyl alcohol–formaldehyde (PVF) has been widely used as a cleaning material and medical dressing because PVF exhibits numerous advantages, including open-cell structure, good mechanical properties at low density, hydrophilicity and excellent biocompatibility[23, 24], Macroporous PVF can be modified to develop novel functions through chemical reactions because of the presence of a large number of hydroxyl groups in a PVF network[25, 26]. In the present study, the macroporous PVF based superabsorbents are obtained through grafting polymerization of hydrophilic acrylamide and successive hydrolysis under basic condition. The related absorption behavior and mechanism are investigated extensively.

Experimental

Materials

Poly (vinyl alcohol) (PVA) powder with a degree of polymerization 2000 and saponification degree of 99% was purchased from Shanxi Sanwei Group Co. Ltd, China. Triton X-100, glutaraldehyde (50% aqueous solution), ceric ammonium nitrate (CAN) and acrylamide (AM) were obtained from Aladdin. Other reagents were purchased from Beijing Chemical Works and used as received.

Preparation of pristine polyvinyl alcohol-formaldehyde (PVF) sponge

A typical preparation of PVF sponge was reported in literature[27, 28]. In detail, a certain amount of PVA was dissolved in 450 g hot water by vigorous stirring with magnetic stir bar at 95^{o}C until completely dissolution. Then, calculated formaldehyde and Triton X-100 were poured into 60 g of hot PVA solution under vigorously stirring. The liquid froths were obtained after 5 min, then 30 mL of H_2SO_4 50 wt% was poured into the above froth at room temperature. After reaching a maximum volume, the froth was poured into a mold and cured in an oven at 60^{o}C for 5 h. The raw sample was washed with water at least for five times to remove unreacted reactants. Finally, the sponge with apparent density of 0.073 g.cm^{-3} was available after drying at 60^{o}C to a constant weight.

Preparation of PVF-GA sponge

Typically, 10 g PVF sponges and 0.52 g GA were added into 400 mL 20 wt% H_2SO_4 aqueous solution. The mixture was sealed and kept at 25 °C for 24 h. Then, the sample was washed with water at least six times to remove sulfuric acid and unreacted GA, and dried at 60 °C to a constant weight. PVF-GA was obtained with an apparent density of 0.071 g.cm^{-3}.

Preparation of macroporous PVF-g-PAM and PVF-g-GAM sponges

Grafting polymerization of acrylamide on the macroporous PVF was carried out using CAN as initiator under nitrogen atmosphere at room temperature. Typically, 2 g (10 mmol) PVF was swollen in 100 mL of 0.01 M nitric acid solution and kept for 0.5 h under nitrogen stream, then 20 mL 0.01 M diluted nitric acid solution dissolved with 0.5483 g (~1 mmol) CAN was added to flask. The initiation reaction was continued for 15 min, then 3.556 g (50 mmol) acrylamide was added to the above mixture under stirring at 25 ^{o}C for 24h, As-prepared samples were washed for six times with deionized water-ethanol mixture to remove unreacted reactants and dried in a vacuum oven at 60 ^{o}C to constant weight, then the PVF-g-PAM-5 was obtained, the PVF-g-PAM-10 can be obtained by increasing the feed amount of acrylamide to 7.112 g (100 mmol). The grafting polymerization of acrylamide on PVF-GA was similar to the above procedure. The result samples were denoted as PVF-g-GAM-5 and PVF-g-GAM-10, respectively. Here, the 5 and 10 donate as feed ratio of [AM]/[OH]. The grafting percentage (*GP*) and grafting efficiency (*GE*) of samples were calculated using gravimetric method according to the flowing equations.

$$GP = (W_2\text{-}W_0)/W_0 \times 100 \qquad (1)$$

$$GE = (W_2\text{-}W_0)/W_1 \times 100 \qquad (2)$$

Where W_0, W_1 were the weights (g) of pristine PVF sponge and monomer of AM, respectively, and W_2 was the weight of PVF-g-PAM after the homopolymer was removed.

The nitrogen content of resultant PVF-g-PAM was measured and the *GP* and *GE* were also calculated according to the following equations (see supporting information).

$$GP = \frac{N\%}{0.197 - N\%} \times 100 \qquad (3)$$

$$GE = \frac{W_2 \times N\%}{0.197W_1} \times 100 \qquad (4)$$

where *N%* was the nitrogen contents in PVF-g-PAM samples.

Preparation of macroporous PVF-g-PAA and PVF-g-GAA sponges

The macroporous PVF-g-PAA and PVF-g-GAA samples were available via the hydrolysis of PVF-g-PAM and PVF-g-GAM in 0.2 M NaOH at 60°C for 6 h. Then, the hydrolyzed samples were washed thoroughly with water-acetone mixture and dried in a vacuum oven at 60°C to a constant weight.

The hydrolysis degree of PVF-g-PAM samples in alkaline solution was examined using elemental analysis and calculated using the following equation (see supporting information).

$$HD = \left(1 - \frac{23 + 14/N\%}{23 + 14/N_1\%}\right) \times 100 \qquad (5)$$

where *N*%, N_1% were the nitrogen contents of as-prepared PVF-g-PAM-n (or PVF-g-GAM-n) and PVF-g-PAA-n (or PVF-g-GAA-n), respectively.

Instruments and Characterization

Fourier transform infrared spectrum was measured on Bruker Vertex 70 spectrometer with attenuated total reflection (ATR) attachment. Solid-state CP/MAS ^{13}C-NMR was carried out on a Bruker AV-400-WB spectrometer. Elementary analysis was run on the Elementary (Vario EL). For Scanning electron microscopy (SEM) test, the dried sponge was cut into sheet and immersed into liquid N_2 for 5 mins, then quickly broken off to get a random brittle-fractured surface and coated with a layer of gold for SEM observation, which were observed through a field-emission environmental SEM (Micro FEI Philips XL-30-ESEM-FEG) operating at 15 and 20 kV. Pore size and

porosity were obtained by an automatic intrusion porosimeter (Autopore IV 9500, Micromeritics, USA). Mechanical properties were evaluated by uniaxial compression tests at 20 °C using the Instron 1121 testing machine (Canton, MA, USA). Rectangular block of the samples with surface dimensions of 50 × 40 mm^2 and with thickness of 20 mm was employed and compressed at a cross-head speed of 5 mm/ min.

Measurement of water absorption performance

The mass method was employed to evaluate the water absorption performance of samples before and after hydrolysis at 25 °C in deionized water and saline solution. At certain time intervals, the samples were taken from the water (deionized water or saline solution) and the weights of wet sponges were determined after being drained for 0.5 min in stainless mesh. The absorption amount at time t was defined as the following formula.

$$Q_t = (W_t - W_2)/W_2 \qquad (6)$$

where W_2 and W_t were the weights of dried and wet samples at time t, respectively. The state of equilibrium swelling could be attained after 10 min and the saturated absorption capacity could be obtained using the following formula.

$$Q_s = (W_s - W_2)/W_2 \qquad (7)$$

where W_2 and W_s were the weights of dried and wet samples at swelling equilibrium state, respectively.

Reusability of water absorption

Reusability test was carried out by simple squeezing using a 500 grams calibration weight, and the absorbed water was collected from sponges. The recovery ($R\%$) of water was calculated as follows:

$$R\%=W_{re}/(W_e-W_0)\times 100 \qquad (8)$$

where W_{re} was the weight of collected water, W_0 is the dry weight of sponge, and W_e is the swollen sample mass at absorption equilibrium state, respectively. The squeezing experiments were performed for 20 cycles for each sample.

Results and Discussion

Characterization of chemical structure of the as-prepared PVF based sponges

To verify the successful grafting and hydrolysis of PAM on the macroporous PVF and the PVF-GA network, the FTIR spectra of sponges are shown in Figure 1. The characteristic peaks at 3200-3600 cm^{-1} and 2843-2943 cm^{-1} of pristine PVF and PVF-GA are attributed to the O–H and C–H stretching vibration of the macroporous network, respectively. PVF-GA, formed by introducing a small amount of GA into the PVF network, presents a nearly identical the same spectrum as the original PVF. After grafting polymerization occurs, PVF-g-PAM-5 and PVF-g-GAM-5 show a strong shoulder at 3200-3600 cm^{-1} and at 1671 cm^{-1} attributed to the –NH and C=O stretching vibration of polyacrylamide, respectively; this result indicates that acrylamide has been grafted onto the PVF and PVF-GA networks. In the hydrolyzed PVF-g-PAA-5 and PVF-g-GAA-5, a new peak at 1571 cm^{-1}corresponding to the C=O stretching vibration of sodium acrylate suggests that sodium polyacrylate is available. The formation of sodium polyacrylate in the network of hydrolyzed samples can also be confirmed from the change of FTIR spectra for pure polyacrylamide and sodium polyacrylate (Fig S2), respectively. Specifically, the bimodal band at 1652 and 1601

cm^{-1} attributed to the C=O stretching vibration and $–NH_2$ bending vibration amide almost disappears in the pure sodium polyacrylate. The existence of the peak at 1671 cm^{-1}, which is attributed to the C=O stretching vibration of acrylamide, confirms the presence of residue amide groups in the hydrolyzed samples. The strong shoulder at 3200 cm^{-1} to 3600 cm^{-1} is probably attributed to the enhancement of hydrogen bonding interactions after hydrolysis reaction occurs under alkaline conditions. Similar results can also be observed in the samples with a high feed ratio of [AM]/[OH] (Figure S1).

Figure 2 shows the solid-state CP/MAS ^{13}C NMR spectra of pristine PVF, PVF-GA, PVF-g-PAM (GAM), and PVF-g-PAA (GAA). The peaks at 84.6 ppm and 101.7 ppm are attributed to methylene C_a of the six-membered-cyclic acetal; the peaks at 58.5-83.8 ppm depict the methine of the PVF network. The peaks at 30-50 ppm correspond to the characteristic peaks of methylene. Compared with the pristine PVF, PVF-g-PAM-5(GAM-5) exhibits a new peak at 179.3 ppm that represents C_b of the amide group, and the intensity of this peak increases with the feed ratio of [AM]/[OH].The appearance of the new peak at 183.9 ppm in PVF-g-PAA-5(GAA-5) corresponds to C_c of the carboxylic group, which is produced when the partly amide group in PVF-g-PAM-5(GAM-5) is hydrolyzed under alkaline condition. The variation of spectra after hydrolyzing can also be confirmed by the pure PAM and sodium polyacrlate (Fig S3), the peak for C of amide at 180.5 ppm shifts to the 185.7 ppm for C of carboxylic group. Compared with the characteristic of the PAM-grafted samples, the partial overlap with the signal of a residue amide indicates that the

PVF-g-PAA-5(GAA-5) is partially hydrolyzed. The spectra of PVF-g-GAM-10 and PVF-g-GAA-10 also exhibit similar characteristic peaks to PVF-g-PAM-10 and PVF-g-PAA-10 (Fig S4), respectively, thus, the introduction of GA into the PVF network almost have no influence on the grafting polymerization and hydrolysis of AM.

Grafting percentage and hydrolysis degree

The CAN has been used as an effective initiator that forms a redox system with alcohols, aldehydes, and amines for grafting polymerization through the disproportionation of coordination complexes in nitric acid media[29-32]. The macroporous PVFs are used as a reducing agent during grafting polymerization (Scheme 1), and the majority of the monomer can be grafted to the PVF and PVF-GA network[33]. Table 1 shows the basic parameters of related samples. The grafting percentage (*GP*) of acrylamide markedly increases with the feed ratio of [AM]/[OH]. For example, the *GP*s of PVF-g-PAM-5 and PVF-g-PAM-10 are 59% and 160%, respectively, and the values calculated from the nitrogen content using elementary analysis are 77% and 130%, respectively. The grafting efficiency (*GE*)*s* of the above two samples are 32% and 44%, respectively, whereas the *GEs* values obtained from elementary analysis are 36% and 39%, respectively. These results indicate that CAN is an efficient initiator for the grafting polymerization of AM onto the PVF network. Notably, the introduction of small amount of GA almost have no influence on the further grafting polymerization of PAM, for example, the GPs of PVF-g-GAM-5 and PVF-g-GAM-10 are 65% and 161%, respectively, and their GEs are 35% and 43%,

respectively. The *GPs* obtained though elementary analysis are 69% and 155%, the *GEs* are 35% and 41%, respectively. These values are similar to those of samples without introducing of GA, therefore, the introduction of GA almost has no influence on the further grafting polymerization. The high grafting efficiency is also determined on the basis of the characteristics of the CAN initiator and PVF. The macroprous and open-cell structure of pristine PVF induces reagents such as CAN, catalyst and acrylamide to penetrate and diffuse into the pores; thus these reagents can effectively facilitate grafting onto the network of PVF.

Hydrolysis is sequentially performed under basic conditions. The hydrolysis degrees of PVF-g-PAA-5, PVF-g-PAA-10, PVF-g-GAA-5 and PVF-g-GAA-10 at 60^{o}C for 6 h are 63.2%, 69.6%, 68.1% and 69.1%, respectively, indicating that the samples with a high hydrolysis degree can be obtained in short time.

Pore structure and porosity

Figure 3 shows the pore size and distribution measured using mercury intrusion porosimeter, and the detailed data are listed in Table 1. PVF and PVF-g-GAM-5 exhibit the average pore size at 60.4 μm, whereas PVF-g-PAM-5 possesses relatively larger pore sizes at 90.7 μm. The hydrolyzed samples, including PVF-g-PAA-5 and PVF-g-GAA-5 possess similar average pore sizes to pure PVF; but PVF-g-GAA-10 yields an average pore size of 90.7 μm. All samples display the high porosity ($\geqslant$86%), which is similar to that of pristine PVF (95.0%). For example, the porosities of PVF-g-PAM-5, PVF-g-PAA-5, PVF-g-GAM-5 and PVF-g-GAA-5 are 87.5%, 92.6%, 86.2% and 93.9%, respectively; these results demonstrate that unique open-cell

structure and high porosity of original PVF are almost remained after successive grafting polymerization and hydrolysis under the alkaline condition. As listed in Table 1, the slight increase of porosity with the feed ratio of [AM]/[OH] is probably attributed to the changes associated with inter- and intra- interactions after the grafting polymerization of AM onto the network. In addition, the porosity of the hydrolyzed samples ranges from 91% to 94% which facilitates rapid water absorption. The samples with high feed ratio of [AM]/[OH] also display similar average pore size and distribution (Fig S5).

The surface morphology are also observed using SEM, as shown in Figure 4. Pore size spans from a few micrometer to 200μm, which is in agreement with a broad pore size distribution from mercury intrusion porosimeter and enlarged view of sponges (Fig S6). All samples exhibit the interconnected pore structures and macroscopically rough surface, which facilitate the penetration of external solvents into the network and will contribute to a quick absorption kinetic process and high absorption capacity.

Absorption kinetics and fitting of kinetic equation

Aqueous solutions, such as deionized water or saline solution are typically selected as testing media for absorption experiments. Figure 5a exhibits the absorption kinetics of the samples in deionized water. The absorption equilibrium of pure PVF is reached in 120 s. By comparison, the absorption equilibrium of PAM-grafted and hydrolyzed samples is reached in 30 s to 60 s. In Figure 5b, pristine PVF, PVF-g-PAM, and PVF-g-GAM in saline solution exhibit similar absorption kinetic curves to those in deionized water. It should be mentioned that the salt ions play an important role in the

absorption process of charged polymer[34, 35], compared with the samples in deionized water, the PVF-g-PAA and PVF-g-GAA in saline solution display relatively rapid absorption rate and reach absorption equilibrium within 30s. The rapid adsorption kinetics of acrylamide-grafted sponge can also be confirmed on the basis of the water absorption performances of PVF, PVF-g-GAM-10 and PVF-g-GAA-10 (Video 1, ESI†). For the pure PVF, a water droplet initially stays on the PVF surface and then penetrates the pore channel in 90 s. By contrast, the water droplet can be absorbed by PVF-g-GAM-10 and PVF-g-GAA-20 once the samples come in contact with water.

The second-order rate expression is used to analyze the swelling behavior of the as-prepared samples, and the absorption rate at any time can be expressed as follows

$$\frac{dQ_t}{dt} = k(Q_s - Q_t)^2 \qquad (9)$$

where Q_t and Q_s are the absorption amounts at time t and at an equilibrium state, respectively, and k is the rate constant. A linear relationship between t/Q_t and t is obtained upon integration.

$$\frac{t}{Q_t} = \frac{1}{kQ_s^2} + \frac{1}{Q_s}t \qquad (10)$$

The experimental points of the samples in deionized water exhibit a perfect straight line with a linear correlation coefficient of $R^2 > 0.99$ (Figure 6), this result indicates that the absorption follows the second-order rate kinetic equation. Q_s and k, which are obtained from the slope and intercept of the straight lines in Figure 6, are summarized in Table 2. In deionized water, the pristine PVF exhibits a relatively slow absorption rate with k of 0.0019 g. g^{-1}. s^{-1}; by contrast, PVF-g-PAM and PVF-g-GAM yield k ranging from 0.0288-0.0948 g. g^{-1}. s^{-1}, which are approximately 15-50 times higher

than those of pristine PVF. These results demonstrate that the grafting polymerization of hydrophilic PAM onto the PVF network effectively accelerate the absorption kinetics. But for the hydrolyzed samples PVF-g-PAA and PVF-g-GAA, the *k* values range from 0.0015 to 0.0043 g. g^{-1}. s^{-1}, which are higher than that of pristine PVF but lower than that of PVF-g-PAM and PVF-g-GAM, the larger volume expansion for charged PVF-g-PAA samples during swelling require longer time to reach an equilibrium.

In saline solution, the *k* of PVF is 0.0027 g. g^{-1}. s^{-1}, whereas that of PVF-g-PAM and PVF-g-GAM are in the range of 0.0228 - 0.0774 g. g^{-1}. s^{-1}, indicating the presence of salt ions practically does not influence the water absorption kinetics. Conversely, the presence of Na^+ and Cl^- ions in saline solution obviously affect the absorption kinetics of hydrolyzed samples. For example, *k* values of PVF-g-PAA and PVF-g-GAA ranges from 0.0103 to 0.0373 g. g^{-1}. s^{-1}, which are similar to *k* of PVF-g-PAM and PVF-g-GAM but higher than that obtained in the deionized water.

In general, the increase in the feed ratio of [AM]/[OH] positively affects absorption kinetics. For example, the *k* values of PVF-g-PAM-5 and PVF-g-PAM-10 in deionized water are 0.0288 and 0.0356 g. g^{-1}. s^{-1}, respectively, this result is due to the increase in surface hydrophilicity with *GP*. A similar pattern can be observed in saline solution. However, the condition of the hydrolyzed samples with charged groups is different. In deionized water, *k* of PVF-g-PAA decreases with the feed ratio of AM from 0.0043 g. g^{-1}. s^{-1} for PVF-g-PAA-5 to 0.0015 g. g^{-1}. s^{-1} for PVF-g-PAA-10; this phenomenon is possible because a longer time is necessary to fill the pores and induce

swelling of the macroporous networks with a higher GP in deionized water, particularly PVF-g-PAA-10, with a great volume expansion. The *k* values of PVF-g-PAA-5 and PVF-g-PAA-10 in saline solution are 0.0138 g. g^{-1}. s^{-1} and 0.0373 g. g^{-1}. s^{-1}, respectively.

With the introduction of GA into the PVF network, PVF-g-GAM displays relatively higher *k* in deionized water and saline solution. For example, the *k* values of PVF-g-GAM-5 and PVF-g-GAM-10 in deionized water are 0.0667 and 0.0948 g. g^{-1}. s^{-1}, respectively, and in saline solution they are 0.328 and 0.0774g. g^{-1}. s^{-1}. PVF-g-GAA-10 exhibits *k* of 0.0024 and 0.0231 g. $g^{-1} \cdot s^{-1}$ in deionized water and saline solution, respectively; these values are similar to or relatively higher than the corresponding values of PVF-g-GAA-5 (approximately 0.0022 and 0.0103 g. g^{-1}. s^{-1}).

Absorption capacity

In general, absorbents with high water uptake exhibit unique advantages in practical applications. The saturated absorption capacities of sorbents are largely determined by chemical composition, crosslinking degree of absorbents, and the solvents characteristics.

The pristine PVF displays the lowest saturated absorption capacity (*Qs*) of 20.0 $g \cdot g^{-1}$ in deionized water, while the introduction of PAM onto the PVF or PVF-GA network enhances the absorption capacity (Figure 7). For example, PVF-g-PAM-5 and PVF-g-PAM-10 in deionized water show Q_s of 35.8 and 41.1 $g \cdot g^{-1}$, respectively. PVF-g-GAM possesses a relatively lower Q_s (25.5$g \cdot g^{-1}$ for PVF-g-GAM-5 and 40.2 $g \cdot g^{-1}$ for PVF-g-GAM-10) than PVF-g-PAM. This difference is due to the slight

increase in the crosslinking degree, which restricts the swelling degree of the polymer network. Compared with the samples before and after grafting polymerization, our results show that the samples after partially hydrolysis under alkaline condition display a higher absorption capacity both in deionized water and saline solution. In the deionized water medium, PVF-g-PAA-5 and PVF-g-PAA-10 yield Q_s of 196.6 and 318.7 $g \cdot g^{-1}$, respectively, and Q_s of PVF-GAA-5 and PVF-g-GAA-10 is 119.1 and 206.9 $g \cdot g^{-1}$, respectively. These results also indicate that the *Qs* of the hydrolyzed sponges increases with the feed ratio of [AM]/[OH] and decreases with the introduction of GA. The higher Q_s of hydrolysis samples is attributed to combination effects, including electrostatic repulsion between COO^- ions on polymer chain, and osmotic pressure difference between interior and exterior of sponge, which originated from freely mobile counter-ions such as Na^+ and H^+ in the network. So the PVF-g-PAA-10 displays rapidly swelling rate and higher swelling degree in deionized water (Video 2, ESI†).

In saline solution, pristine PVF, PVF-g-PAM-5, PVF-g-PAM-10, PVF-g-GAM-5 and PVF-g-GAM-10 yield Q_s of 21.2, 35.0, 44.1, 23.1 and 40.8 $g \cdot g^{-1}$, respectively, indicating that these five samples exhibit similar swelling behaviors in deionized water and saline solution which is attributed to presence of salt ions almost have no influences on the swelling degree of the neutral polymer network. Compared with the case in deionized water, the Q_ss of PVF-g-PAA-5, PVF-g-PAA-10, PVF-g-GAA-5 and PVF-g-GAA-10 in saline solution obviously decrease to 86.7, 97.3, 64.5 and 91.3 $g \cdot g^{-1}$, respectively. This result is attributed to the charge screen effect of cation on the

-COO^- of the polymer chain, which decrease electrostatic repulsion between COO^- ions as well as osmotic pressure difference between the charged polymer chain and the external solution. Notably, the Q_ss of hydrolyzed samples in saline solution is similar to or higher than that of most absorbents reported in previous studies [36-40].

Reusability

The reusability of traditional gel-based superabsorbents is difficult to be realized through simple squeezing, centrifugation, and other conventional techniques because of diffusion control. In our study, PVF-g-PAM-5 with moderate *GP* is selected to demonstrate reusability. The amount of water absorbed by the sponges is removed easily through simple squeezing (Figure 8). The absorption capacity is practically maintained at 42 $g \cdot g^{-1}$ to 43 $g \cdot g^{-1}$, and recovery remains at 87% to 88% for 20 absorption–squeezing cycles; this result indicates excellent reusability. Such excellent reusability and recovery are attributed to good mechanical properties, open-cell structure, and high swelling in water. In addition, the squeezed PVF-g-PAM-5 can reach the saturated absorption rapidly upon contact with water. Only PVF-based sponges with an absorption capacity less than 50 $g \cdot g^{-1}$ exhibit excellent reusability because sponges with high absorption capacity generally possess low mechanical properties and weak anti-squeezing ability. Therefore, these hydrophilic and macroporous PVF-based sponges are considered as new candidates of water superabsorbents in practical applications.

The excellent reusability of PVF-g-PAM-5 is attributed to its good mechanical properties at dried state and good residence at swollen states. As shown in Figure 9,

the dried PVF-g-PAM-5 displays representative trend of porous material, which composite plateau region and densification regime. The Young's modulus is 2.58±0.12 MPa and maximum load at strain of 75% is 2.39±0.12 MPa, respectively, indicating its good mechanical properties. As the water molecular act as plasticizer and the solvation effect of grafted PAM chain, the swollen sample is supersoft (inset in Figure 9), for example, the Young's modulus of sample at the first cycle is 6.47±0.20 KPa while that of second compression is 6.85±0.44 KPa, these results demonstrate that the swollen sample displays good squeezing repeatability.

Absorption mechanism

The rapid absorption kinetics of PAM-grafted and -hydrolyzed PVF sponges is mainly attributed to the hydrophilic surface and macroporous open-cell structure. In particular, the hydrophilic surface and interconnected pore structure induce the water molecule to quickly wet the surface and then penetrate into the network of sponges in a few seconds because the characteristic size of the cell wall is in micrometer[12] The water absorption capacity of porous polymers is decided by the porosity and swelling degree of sponge in the water. The amphiphilic neutral network of the original PVF restricts the swelling of polymer chains. By contrast, the solvation effect of the hydrophilic polyacrylamide in PVF-g-PAM or PVF-g-GAM can slightly enhance the swelling degree of the samples in water; this value increases with the *GP* of polyacrylamide in the samples. However, in PVF-g-PAA and PVF-g-GAA sponges containing a polyelectrolyte component in their networks, the repulsion effect of sodium polyacrylate and the osmotic pressure difference between the internal network and the

external solution are the two key factors that determine the solvation degree of polyelectrolyte and the swelling degree of samples in the water medium. These two factors (repulsion effect of sodium polyacrylate and the osmotic pressure) decrease with the appearance and concentration of the electrolyte in the water medium, the electrolyte can shield the interaction between the charge groups on polymer chains and decrease the difference of osmotic pressure. As a consequence, the Q_ss in saline solution decrease rapidly compared with those in deionized water. The high porosity of sponges also positively affects the increase in water absorption capacities by filling the pores.

Conclusions

Macroporous and hydrophilic PVF-based sponges are effectively prepared through the grafting polymerization of polyacrylamide on the PVF sponge by using CAN as a redox initiator and through the partial hydrolysis under alkaline condition. The main results are summarized as follows:

I. The *GP* increases with the feed ratio of [AM]/[OH] and can reach up to 160% while the introduction of GA has almost no influence on the *GP* and *GE*. The hydrolysis degree ranges from 60% to 70%.

II. The as-prepared grafted and hydrolized sponges exhibit interconnected pore structure, macroscopically rough surface, high porosity of 90%, and pore size ranging from several micrometers to 200 μm.

III. As-prepared PVF-based sponges display extremely rapid absorption kinetics and can reach absorption equilibrium within 1 minute in both deionized water

and saline solution because of the hydrophilic surface, high porosity and interconnected pore structure. The absorption described in this study fits the pseudo second-order rate kinetic equation.

IV. PVF-g-PAA sponges can absorb deionized water to a high extent of 320g·g^{-1} in 60 s and can also absorb saline solution up to 97.3 g·g^{-1} within 30 s.

V. The as-prepared PVF-g-PAM sponges with absorption capacity less than 50g·g^{-1} exhibit excellent reusability at least for 20 cycles which is realized only through a simple squeezing.

VI. The excellent water absorption performance of PVF-g-PAM(PAA) sponges is attributed to the combined effect of open-cell structure, high porosity, hydrophilic surface as well as the presence of osmotic pressure and electrostatic repulsion between the COO^- ions in the hydrolyzed sponge.

VII. These sponges with rapid absorption kinetics and high absorption capacity can be used as new candidates of superabsorbents for medical and sanitary applications.

ACKNOWLEDGEMENTS

This research was supported by National Natural Science Foundation of China (General: 51173180) and Department of Science and Technology of Jilin Province (20130206057GX).

AUTHOR INFORMATION

Corresponding Author

***E-mail:** xlji@ciac.ac.cn

SUPPORTING INFORMATION

Supporting information is available for this article, with the following content:

Video 1: Water absorption process of samples

Video 2:Swelling of PVF-g-GAA 10 in water

The formula derivation of *GP* and *GE* from the nitrogen contents; the FTIR, solid-state CP/MAS ^{13}C-NMR and pore size distribution of sponge with high feed ratio of [AM]/[OH]

References

1. H. Meng, P. Xiao, J. C. Gu, X. F. Wen, J. Xu, C. Z. Zhao, J. W. Zhang and T. Chen, *Chemical Communications*, 2014, 50, 12277-12280.
2. P. Liu, L. Jiang, L. Zhu and A. Wang, *Industrial & Engineering Chemistry Research*, 2014, 53, 4277-4285.
3. B. Jeong, K. M. Lee, A. Gutowska and Y. H. An, *Biomacromolecules*, 2002, 3, 865-868.
4. A. S. Hoffman, *Advanced Drug Delivery Reviews*, 2012, 64, Supplement, 18-23.
5. M. Köllmer, V. Keskar, T. G. Hauk, J. M. Collins, B. Russell and R. A. Gemeinhart, *Biomacromolecules*, 2012, 13, 963-973.
6. K. L. Spiller, S. J. Laurencin, D. Charlton, S. A. Maher and A. M. Lowman, *Acta Biomaterialia*, 2008, 4, 17-25.
7. S. G. Levesque, R. M. Lim and M. S. Shoichet, *Biomaterials*, 2005, 26, 7436-7446.
8. Q. Liu, E. L. Hedberg, Z. Liu, R. Bahulekar, R. K. Meszlenyi and A. G. Mikos, *Biomaterials*, 2000, 21, 2163-2169.
9. J. Chen, H. Park and K. Park, *Abstracts of Papers of the American Chemical Society*, 1998, 216, U832-U832.
10. H. Omidian, J. G. Rocca and K. Park, *Journal of Controlled Release*, 2005, 102, 3-12.
11. D. Kim and K. Park, *Polymer*, 2004, 45, 189-196.
12. J. Chen, H. Park and K. Park, *Journal of Biomedical Materials Research*, 1999, 44, 53-62.
13. S.-L. Loo, W. B. Krantz, T.-T. Lim, A. G. Fane and X. Hu, *Soft Matter*, 2013, 9, 224-234.
14. J. Chen and K. Park, *Journal of Controlled Release*, 2000, 65, 73-82.
15. S. Chaterji, I. K. Kwon and K. Park, *Progress in Polymer Science*, 2007, 32, 1083-1122.
16. J. H. Kim, S. B. Lee, S. J. Kim and Y. M. Lee, *Polymer*, 2002, 43, 7549-7558.
17. Y. Chen, Y.-f. Liu, H.-m. Tan and J.-x. Jiang, *Carbohydrate Polymers*, 2009, 75, 287-292.
18. G. R. Mahdavinia, A. Pourjavadi, H. Hosseinzadeh and M. J. Zohuriaan, *European Polymer Journal*, 2004, 40, 1399-1407.
19. J. Wu, Y. Wei, J. Lin and S. Lin, *Polymer*, 2003, 44, 6513-6520.
20. X. Shi, W. Wang and A. Wang, *Journal of Polymer Research*, 2011, 18, 1705-1713.
21. X.-N. Shi, W.-B. Wang and A.-Q. Wang, *Colloids and Surfaces B-Biointerfaces*, 2011, 88, 279-286.
22. W. Wang and A. Wang, *Carbohydrate Polymers*, 2009, 77, 891-897.
23. H.-B. Chen, E. Hollinger, Y.-Z. Wang and D. A. Schiraldi, *Polymer*, 2014, 55, 380-384.
24. O. Okay and V. Lozinsky, in *Polymeric Cryogels*, ed. O. Okay, Springer International Publishing, 2014, vol. 263, ch. 3, pp. 103-157.
25. Y. Pan, W. Wang, C. Peng, K. Shi, Y. Luo and X. Ji, *RSC Advances*, 2014, 4, 660-669.
26. Y. Pan, C. Peng, W. Wang, K. Shi, Z. Liu and X. Ji, *RSC Advances*, 2014, 4, 35620-35628.
27. H. G. Hammond, *US 2668153,* 1953.
28. Y. Pan, K. Shi, C. Peng, W. Wang, Z. Liu and X. Ji, *ACS Applied Materials & Interfaces*, 2014, 6, 8651-8659.
29. F. R. Duke and A. A. Forist, *Journal of the American Chemical Society*, 1949, 71, 2790-2792.
30. M. D. Fernández, T. Fernández, M. J. Fernández and G. M. Guzmán, *Journal of Polymer Science: Polymer Chemistry Edition*, 1984, 22, 2729-2732.
31. G. G. Guilbault and W. H. McCurdy, *The Journal of Physical Chemistry*, 1963, 67, 283-285.

32. G. Mino, S. Kaizerman and E. Rasmussen, *Journal of the American Chemical Society*, 1959, 81, 1494-1496.
33. B. Gao, J. Lu, R. Zhuang and G. Zhang, *Journal of Applied Polymer Science*, 2009, 114, 3487-3494.
34. J. Li, Z. Suo and J. J. Vlassak, *Journal of Materials Chemistry B*, 2014, 2, 6708-6713.
35. G. Mahdavinia, A. Pourjavadi, H. Hosseinzadeh and M. Zohuriaan, *European Polymer Journal*, 2004, 40, 1399-1407.
36. Y. Bao, J. Ma and N. Li, *Carbohydrate Polymers*, 2011, 84, 76-82.
37. J. Li, J. Ji, J. Xia and B. Li, *Carbohydrate Polymers*, 2012, 87, 757-763.
38. Z.-Q. Zhu, H.-X. Sun, X.-J. Qin, L. Jiang, C.-J. Pei, L. Wang, Y.-Q. Zeng, S.-H. Wen, P.-Q. La and A. Li, *Journal of Materials Chemistry*, 2012, 22, 4811-4817.
39. F. Jiang and Y.-L. Hsieh, *Journal of Materials Chemistry A*, 2014.
40. V. P. S. Nykanen, A. Nykanen, M. A. Puska, G. G. Silva and J. Ruokolainen, *Soft Matter*, 2011, 7, 4414-4424.

Figure captions:

Scheme 1. Synthetic route of PAM grafted and hydrolyzed PVF sponges.

Figure 1. FTIR spectra of pristine PVF, PVF-GA, PVF-g-PAM-5, PVF-GAM-5, PVF-g-PAA-5 and PVF-g-GAA-5.

Figure 2. Solid-state CP/MAS ^{13}C NMR spectra of pristine PVF, PVF-GA, PVF-g-PAM-5, PVF-GAM-5, PVF-g-PAA-5 and PVF-g-GAA-5 at 25 ^{o}C.

Figure 3. Pore size distributions of PVF, PVF-GA, PVF-g-PAM-5, PVF-GAM-5, PVF-g-PAA-5 and PVF-g-GAA-5

Figure 4. SEM images of PVF samples, (a) Pristine PVF, (b) PVF-GA (c-1) PVF-g-PAM-5, (c-2) PVF-g-PAA-5, (d-1) PVF-g-PAM-10, (d-2) PVF-g-PAA-10, (e-1) PVF-g-GAM-5, (e-2) PVF-g-GAA-5, (f-1) PVF-g-GAM-10 and (f-2) PVF-g-GAA-10.

Figure 5. Absorption amount of different sponges in (a) deionized water and (b) saline solution with contact time.

Figure 6. Linear regression of different sponges in (a) deionized water and (b) saline solution using pseudo second-order rate kinetic equation.

Figure 7. Absorption capacity of various sponges in deionized water and saline solution.

Figure 8. Repeated absorption capacity and recovery of PVF-g-PAM-5 in deionized water with cycle number.

Figure 9. Compressive stress–strain curves of PVF-g-PAM-5 at dried state; inset corresponding to the curves at the swollen state.

Table 1. Basic parameters of grafted PVF sponges

Table 2. Swelling behavior of grafted PVF sponges

Table of contents (TOC)

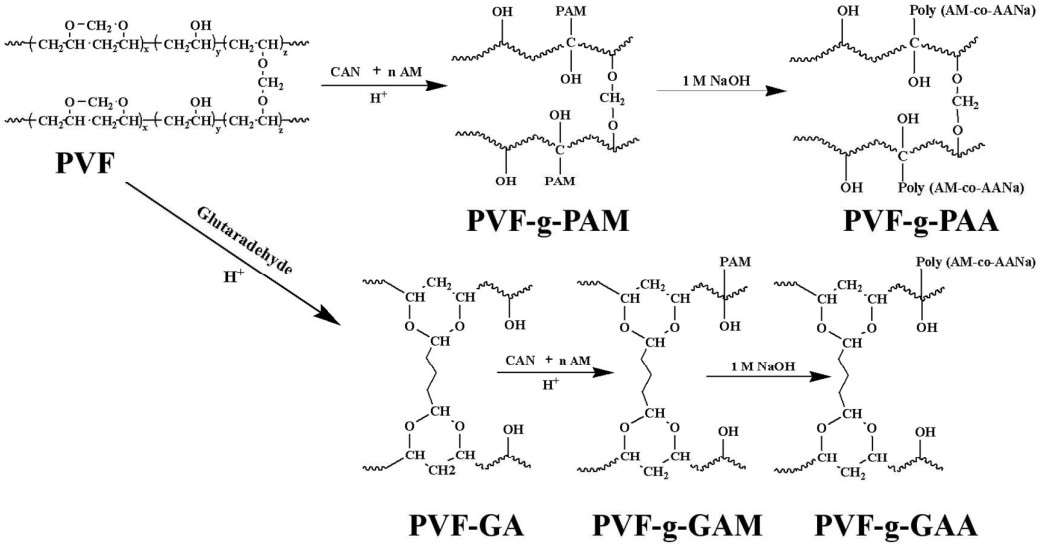

Scheme 1. Synthetic route of PAM grafted and hydrolyzed PVF sponges.

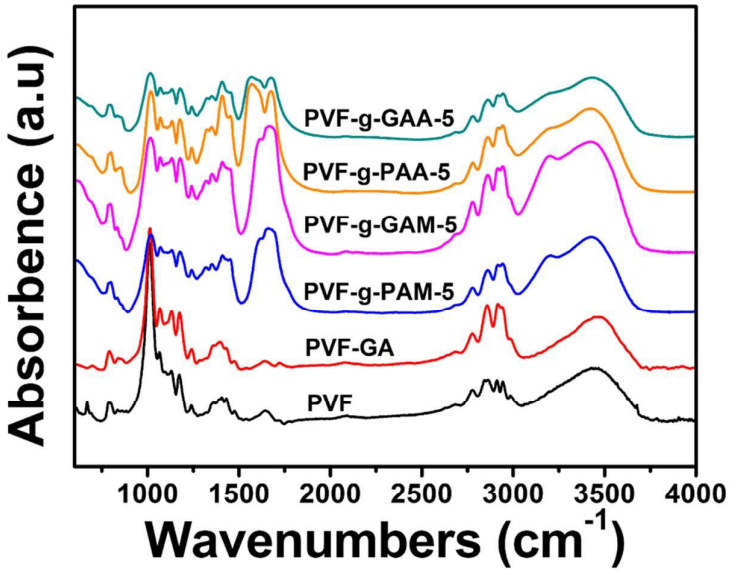

Figure 1. FTIR spectra of pristine PVF, PVF-GA, PVF-g-PAM-5, PVF-GAM-5, PVF-g-PAA-5 and PVF-g-GAA-5.

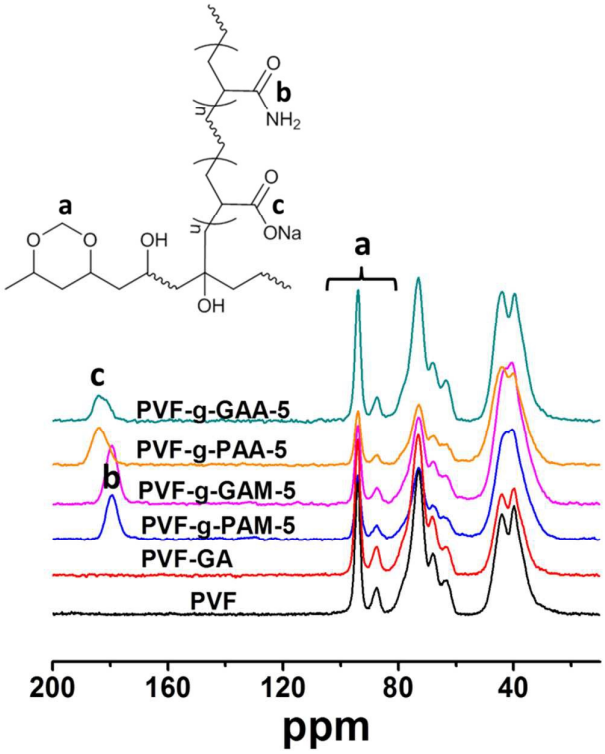

Figure 2. Solid-state CP/MAS ^{13}C NMR spectra of pristine PVF, PVF-GA, PVF-g-PAM-5, PVF-GAM-5, PVF-g-PAA-5 and PVF-g-GAA-5 at 25 ^{o}C.

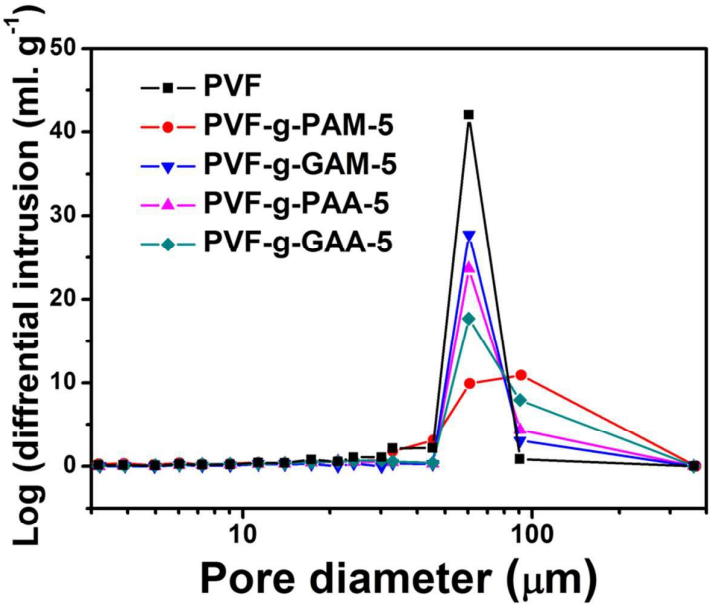

Figure 3. Pore size distributions of PVF, PVF-g-PAM-5, PVF-GAM-5, PVF-g-PAA-5 and PVF-g-GAA-5

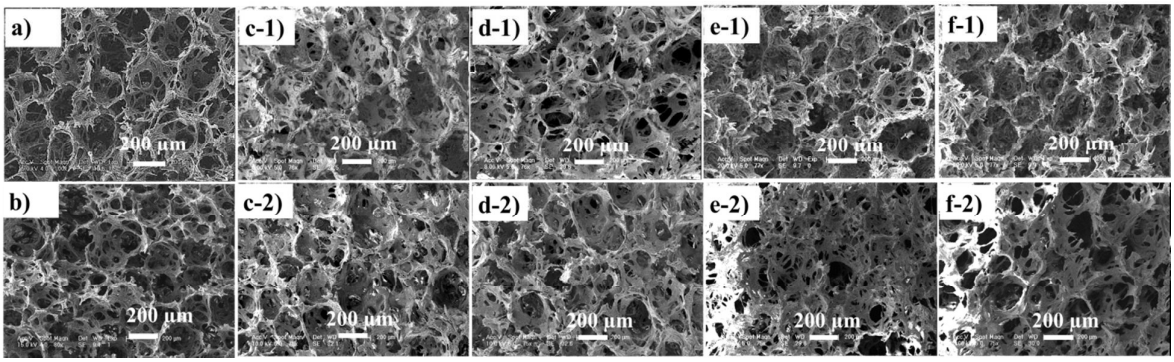

Figure 4. SEM images of PVF samples, (a) Pristine PVF, (b) PVF-GA (c-1) PVF-g-PAM-5, (c-2) PVF-g-PAA-5, (d-1) PVF-g-PAM-10, (d-2) PVF-g-PAA-10, (e-1) PVF-g-GAM-5, (e-2) PVF-g-GAA-5, (f-1) PVF-g-GAM-10 and (f-2) PVF-g-GAA-10.

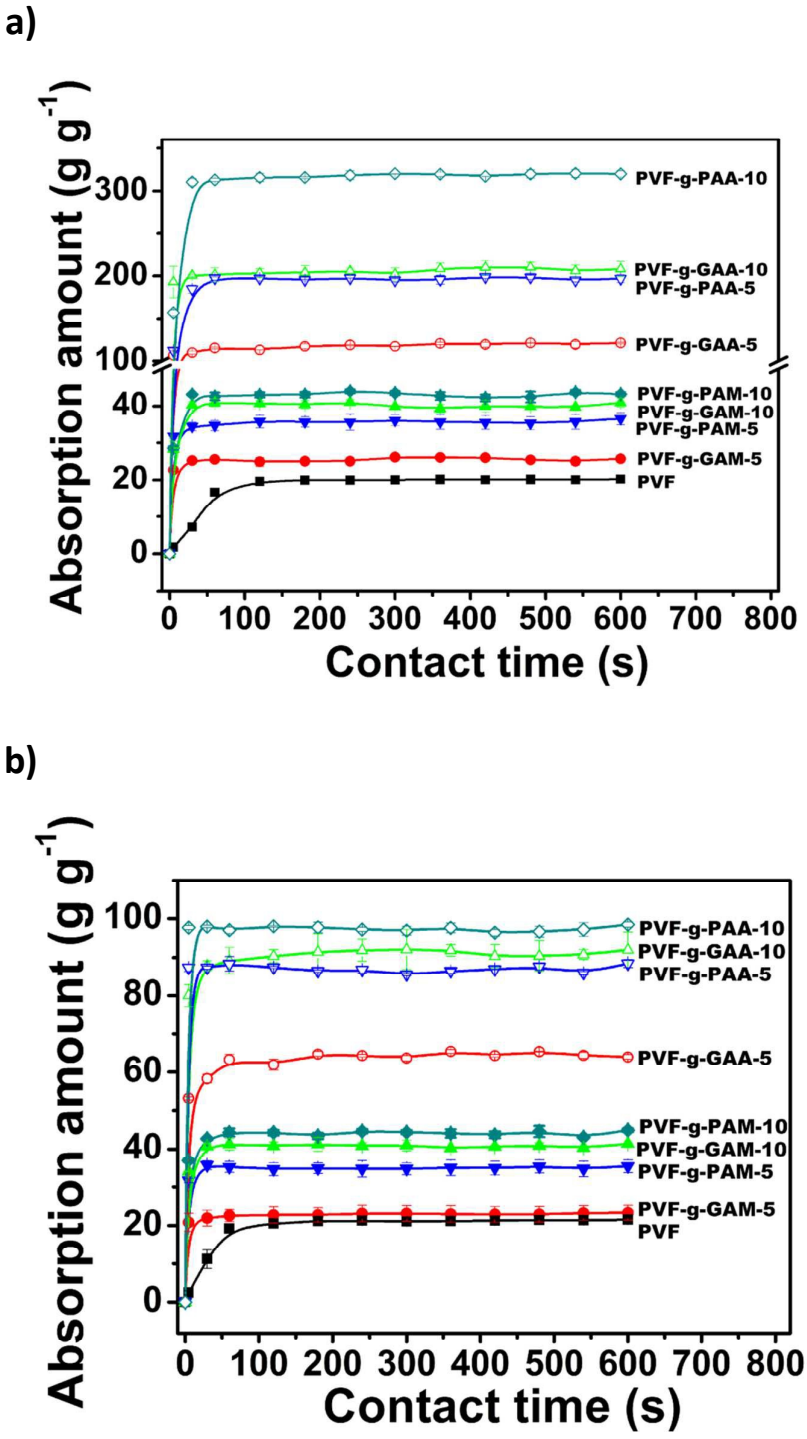

Figure 5. Absorption amount of different sponges in (a) deionized water and (b) saline solution with contact time.

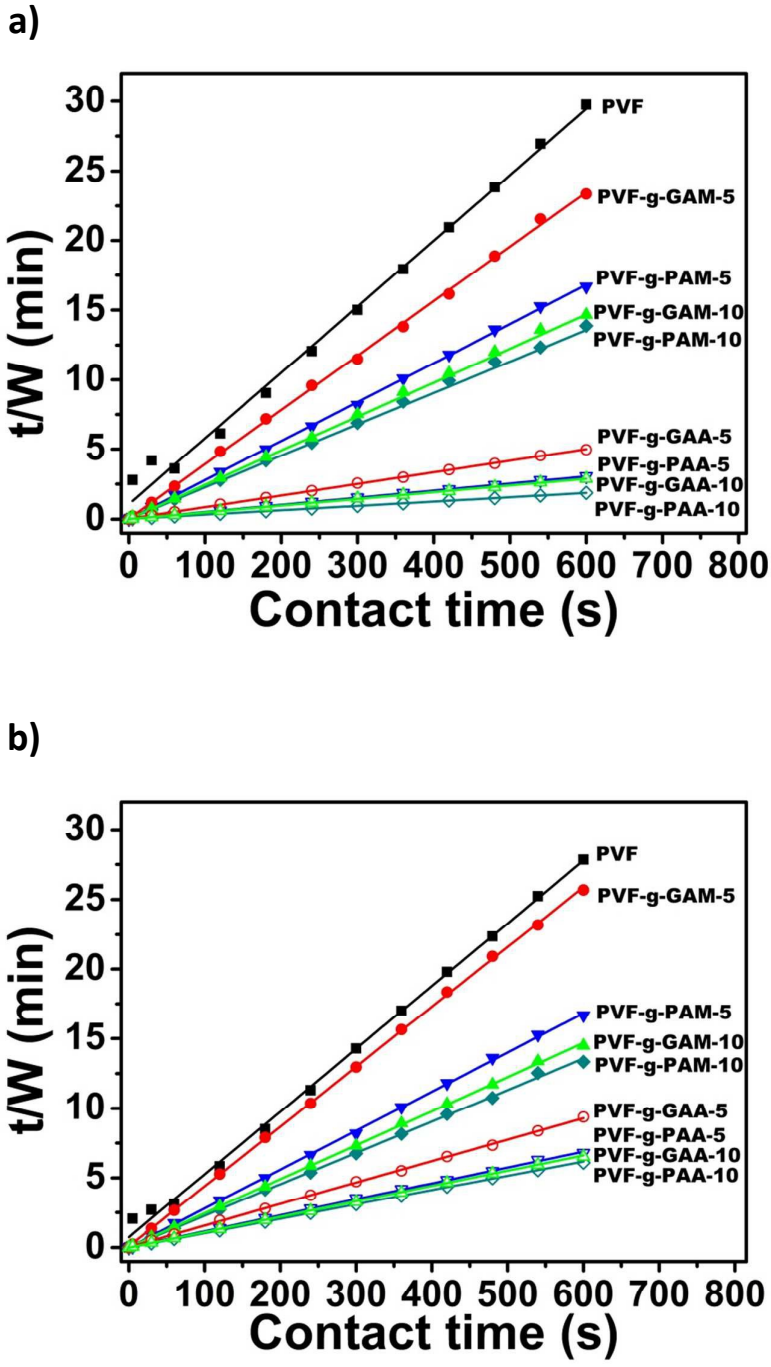

Figure 6. Linear regression of different sponges in (a) deionized water and (b) saline solution using pseudo second-order rate kinetic equation.

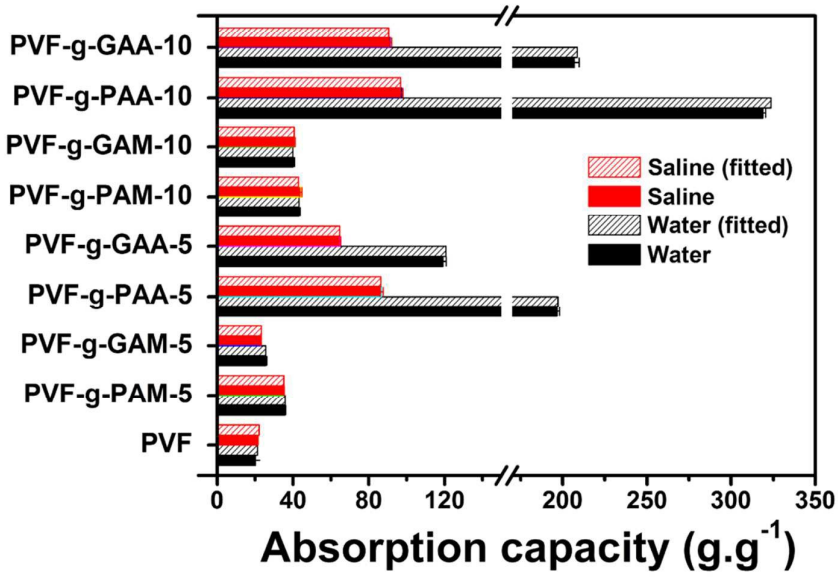

Figure 7. Absorption capacity of various sponges in deionized water and saline solution.

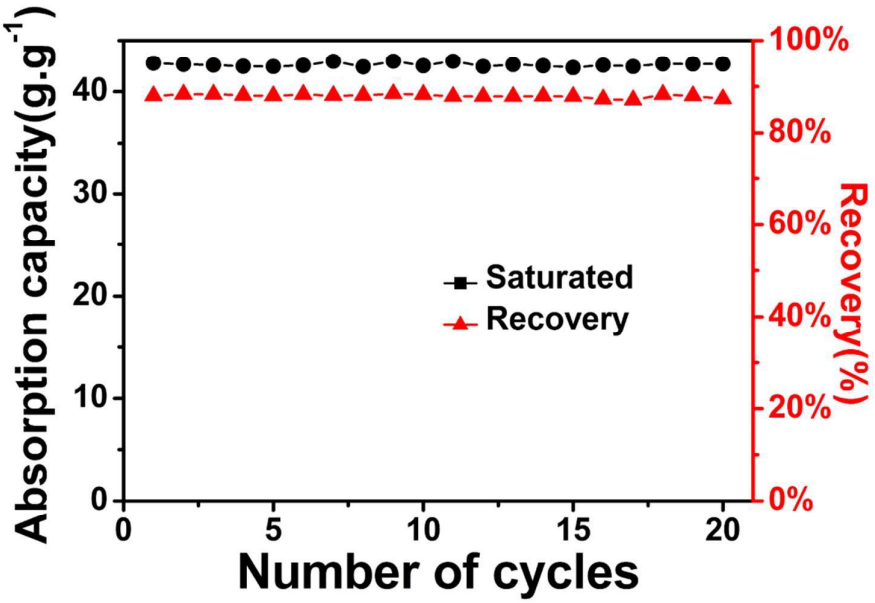

Figure 8. Repeated absorption capacity and recovery of PVF-g-PAM-5 in deionized water with cycle number.

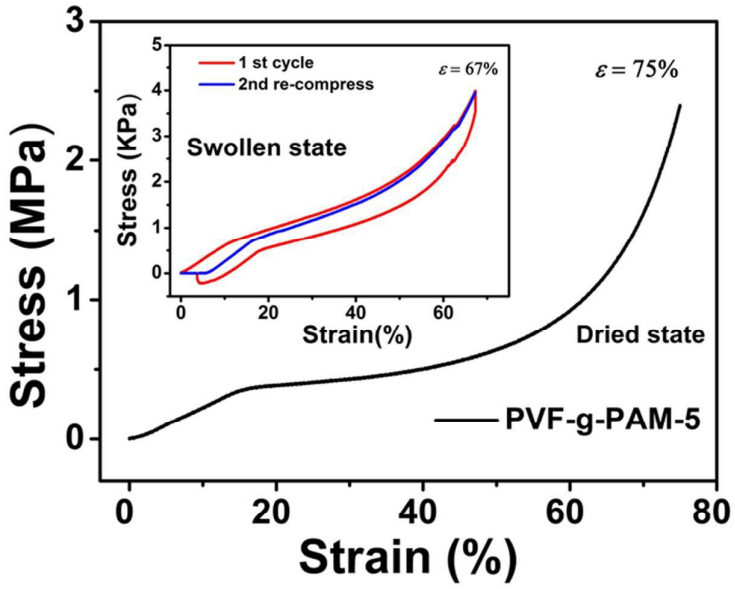

Figure 9. Compressive stress–strain curves of PVF-g-PAM-5 at dried state; inset corresponding to the curves at the swollen state.

Table 1. Basic parameters of grafted PVF sponges

Before hydrolysis						After hydrolysis		
Samples	Porosity (%)	GP^1 (%)	GP^2 (%)	GE^1 (%)	GE^2 (%)	Samples	Porosity (%)	Hydrolysis degree (%)
PVF	95.0	——	——	——	——	——	——	——
PVF-g-PAM-5	87.5	59	77	32	36	PVF-g-PAA-5	92.6	63.2
PVF-g-PAM-10	94.7	160	132	44	39	PVF-g-PAA-10	91.1	69.6
PVF-g-GAM-5	86.2	65	69	35	35	PVF-g-GAA-5	93.9	68.1
PVF-g-GAM-10	90.6	161	155	43	41	PVF-g-GAA-10	92.7	69.1

* 1 Calculated using gravimetric method, 2 calculated using elementary analysis.

Table 2. Swelling behavior of grafted PVF sponges

Samples	Deionized water			Saline solution		
	Q_s (g. g^{-1})	k(g. g^{-1}. s^{-1}.)	R^2	Q_s	k(g. g^{-1}. s^{-1})	R^2
PVF	21.2	0.0019	0.9933	22.2	0.0027	0.9975
PVF-g-PAM-5	35.8	0.0288	0.9998	35.2	0.0298	0.9998
PVF-g-PAM-10	43.1	0.0356	0.9995	42.9	0.0420	0.9992
PVF-g-GAM-5	25.6	0.0667	0.9993	23.2	0.0328	0.9998
PVF-g-GAM-10	39.8	0.0948	0.9995	40.5	0.0774	0.9997
PVF-g-PAA-5	197.2	0.0043	0.9998	86.4	0.0138	0.9996
PVF-g-PAA-10	323.6	0.0015	0.9999	96.8	0.0373	0.9998
PVF-g-GAA-5	120.8	0.0022	0.9997	64.6	0.0103	0.9997
PVF-g-GAA-10	208.8	0.0024	0.9997	90.5	0.0231	0.9998

TOC